



HAL
open science

Numerical and experimental assessment of functional beamforming for source quantification

Valentin Baron, Arthur Finez, Barbara Nicolas

► **To cite this version:**

Valentin Baron, Arthur Finez, Barbara Nicolas. Numerical and experimental assessment of functional beamforming for source quantification. BeBeC 2018 -7th Berlin Beamforming Conference, Mar 2018, Berlin, Germany. hal-01729300

HAL Id: hal-01729300

<https://hal.science/hal-01729300>

Submitted on 12 Mar 2018

HAL is a multi-disciplinary open access archive for the deposit and dissemination of scientific research documents, whether they are published or not. The documents may come from teaching and research institutions in France or abroad, or from public or private research centers.

L'archive ouverte pluridisciplinaire **HAL**, est destinée au dépôt et à la diffusion de documents scientifiques de niveau recherche, publiés ou non, émanant des établissements d'enseignement et de recherche français ou étrangers, des laboratoires publics ou privés.



NUMERICAL AND EXPERIMENTAL ASSESSMENT OF FUNCTIONAL BEAMFORMING FOR SOURCE QUANTIFICATION

Valentin Baron¹⁻²⁻³, Arthur Finez¹ and Barbara Nicolas²

¹MicrodB

Chemin du Petit Bois, 69134, Ecully, France

²CREATIS, Univ Lyon, INSA-Lyon, Université Claude Bernard Lyon 1, UJM-Saint Etienne,
CNRS, Inserm, CREATIS UMR 5220, U1206, LYON, France

³Univ. Grenoble Alpes, CNRS, Grenoble INP*, GIPSA-lab,
38000 Grenoble, France

Abstract

Functional Beamforming is an advanced sound source localisation method which improves both spatial resolution and dynamic range compared to conventional beamforming. While it is clear that localisation results are outperformed, uncertainty remains about quantification performances. This article evaluates the quality of the identified acoustic power as a function of the exponent parameter ν . Simulated test cases are set to evaluate the robustness of the method against uncorrelated noise, propagation model errors and extended sources. Then experiments in a controlled environment are carried out to confirm the trends observed previously. Conclusions are that model errors are critical even for low ν which makes this method not suited for quantification studies. However the method is more robust against uncorrelated added noise.

1 INTRODUCTION

Functional Beamforming (FBF) is a microphone array technique introduced by Dougherty [2] in 2014. It is a promising method for acoustic source localization. Basically its idea is to stretch the array response obtained by Conventional Beamforming (CBF) in order to improve the dynamic range. Several studies exhibit the improvements of source localization using this algorithm

*Institute of Engineering Univ. Grenoble Alpes

[7, 8]. However only one [1] to our knowledge deals with the quantification performances, *ie* the level of confidence of the obtained acoustic power levels. In it Chu *et al.* show that FBF affects the obtained source levels in practical situations and they propose corrections to improve them.

The main topic of this contribution is to isolate and understand the causes of these quantification errors. This is performed with simulations reproducing real source errors. Their results are compared to real experimental data to see if the trends observed are conserved.

Section 2 describes FBF. In Section 3 the simulation approach is introduced and its results are shown to validate the quantification losses when using FBF. Finally experimental data are processed in Section 4 and a conclusion is given.

2 METHODS

2.1 Conventional Beamforming

To perform CBF, a grid of potential sources is scanned point by point assuming that every node is a possible location for an acoustic source. CBF theoretically works just for a unique source within the grid. In practice several sources can be present and the localization result remains robust whereas the quantitative one does not. To perform CBF in the frequency domain, recorded pressure signals are transformed into the Fourier domain by short term Fourier transform on temporal snapshots. For a given frequency these Fourier coefficients are concatenated within a pressure vector $\mathbf{p} = [p_1 \cdots p_M]$ where M stands for the number of microphones of the array. The grid and the obtained pressures are represented in Fig. 1.

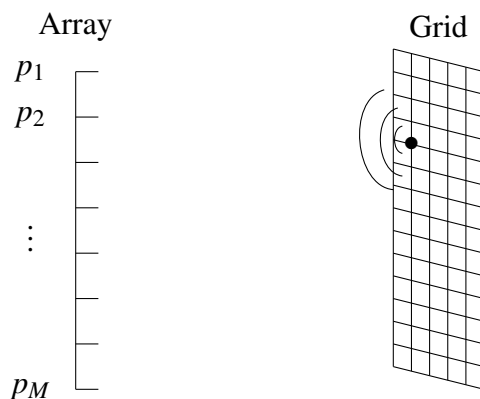


Figure 1: The array processing configuration

This pressure vector is used to estimate the Cross Spectral Matrix (CSM) $C = \langle \mathbf{p}\mathbf{p}^* \rangle$ where $\langle \cdot \rangle$ stands for the ensemble average over temporal snapshots.

Steering vectors \mathbf{g} are built for each grid location. Their values represent a model of propagation between this grid point and each of the array's microphone. Finally the beamforming consists in analyzing the quadratic form composed by this steering vector and the CSM matrix according to Eq. 1 for every grid point.

$$CBF_{\mathbf{g}} = \frac{\mathbf{g}_n^* C \mathbf{g}_n}{\|\mathbf{g}\|_2^2} \quad (1)$$

In Eq. (1) \mathbf{g} represents the steering vector for a given position of the scanned grid and $\mathbf{g}_n = \frac{\mathbf{g}}{\|\mathbf{g}\|_2}$ is the normalized steering vector. The normalization used in CBF depends only on the propagation model. Nevertheless they can be modified like in adaptive beamforming algorithms [3, 9] or Capon's method [4, 5]. These methods are designed to improve localization by taking into account the data in the process. However the simplicity of the CBF allows a better robustness.

2.2 Functional Beamforming

The FBF method is a modification of CBF in two ways using an exponent ν :

- First, the CSM is raised to the power $1/\nu$: $C_{1/\nu} = U S^{1/\nu} U^*$ with U the unitary matrix obtained by Eigen Value Decomposition (EVD) of C and S the diagonal one.
- Second, the quadratic form is raised to the power ν leading to:

$$FBF_{\mathbf{g}} = \frac{(\mathbf{g}_n^* C_{1/\nu} \mathbf{g}_n)^\nu}{\|\mathbf{g}\|_2^2} \quad (2)$$

For illustration purpose, Fig. 2 shows a comparison between results obtained by FBF using different values of ν . This is a 1D case where a single source of frequency 1500 Hz and unitary amplitude is placed on the scan grid at $x = 0$ m without any added noise nor model error.

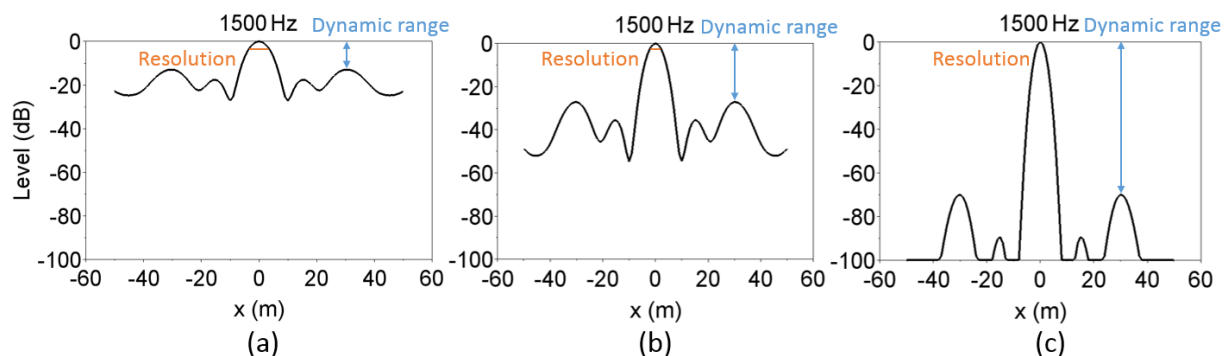


Figure 2: FBF on a single source ($x = 0$ m) in a 1D case for a: $\nu = 1$ (CBF), b: $\nu = 2$ and c: $\nu = 5$

First all the cases recover the acoustic power as for a unitary source it must be 0 dB as observed. Then the dynamic range, defined as the difference between the source level and the maximum of the side lobes, increases with ν from around 15 dB for $\nu = 1$ to 70 dB for $\nu = 5$. Furthermore the resolution, defined as the width of the main lobe at -3 dB, decreases passing from around 8 m to 2 m. So the localization improvements promised by the method are clearly observed in this simulation.

The success of the method lies in the perfect matching between steering vector and the propagation function in this example. In the next subsection an analysis is established over the perturbations that can occur in practice.

2.3 Theoretical Analysis

Perfect match between steering and propagation vector

Let us consider a unique source without model error. \mathbf{g}_i is the steering vector at the position i of the grid and \mathbf{h}_s is the vector describing the physical propagation between the source and the microphones. In the simulated case, by calling s the position of the source within the grid, $\mathbf{g}_s = \mathbf{h}_s$. Taking the example of a unique monopole source of amplitude A , the recorded pressure vector is $\mathbf{p}_s = A \mathbf{h}_s$ and the cross spectral matrix is $C = A^2 \mathbf{h}_s \mathbf{h}_s^*$. Both CBF and FBF's goal is to estimate the acoustic power of the source s defined by its squared amplitude A^2 . Then for the grid point s where the source is located the CBF is:

$$CBF_{\mathbf{g}_s} = \frac{\mathbf{g}_{sn}^* A^2 \mathbf{h}_s \mathbf{h}_s^* \mathbf{g}_{sn}}{\|\mathbf{g}_s\|_2^2} = A^2 \quad (3)$$

Concerning the the FBF, the EVD gives $C = USU^*$ where the first column of U is $\mathbf{h}_s / \|\mathbf{h}_s\|_2 = \mathbf{h}_{sn}$. S has a single non-zero diagonal value equal to $A^2 \|\mathbf{h}_s\|_2^2$. Combining this decomposition within the FBF formula (2) gives:

$$FBF_{\mathbf{g}_s} = \frac{(\mathbf{g}_{sn}^* \mathbf{h}_{sn} A^{2/\nu} \|\mathbf{h}_s\|_2^{2/\nu} \mathbf{h}_{sn}^* \mathbf{g}_{sn})^\nu}{\|\mathbf{g}_s\|_2^2} = \frac{A^2 \|\mathbf{h}_s\|_2^2}{\|\mathbf{g}_s\|_2^2} = A^2 \quad (4)$$

So both CBF and FBF succeed in restoring the source power in the case of a unique source without model error.

Misalignment

In many practical cases, the steering vector does not match perfectly with the physical propagation vector, either because of acoustic reflection, refraction not perfectly controlled or simply because there is no grid point at the "exact" location of the source. The misalignment between the scanning steering vector and the propagation vector is investigated by the simulations in Section 3. A meaningful indicator of this misalignment is the coherence index I_{coh} (Eq. 5). This index can quantify the error made when the source is not perfectly steered by the steering vector.

$$I_{coh}(\mathbf{g}, \mathbf{h}_s) = \cos^2(\theta) = \frac{|\mathbf{g}^* \mathbf{h}_s|^2}{\|\mathbf{g}\|^2 \|\mathbf{h}_s\|^2} \quad (5)$$

Indeed I_{coh} quantifies the angle θ between \mathbf{g} and \mathbf{h}_s as illustrated in the simplified view of Fig.3. Simulations can be carried out to study the impact of this misalignment and this is the purpose of Section 3.

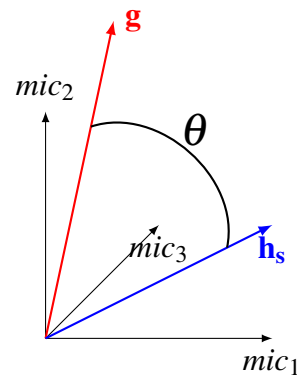


Figure 3: Steering and propagation vector link into the microphone coordinates system

3 SIMULATION

3.1 Simulation Configuration

The simulation setup (Fig. 4) consists in an underwater acoustic case with a linear scan grid of 100 m width and 1 m step size. The source is located at the center of this line and the antenna is a 4.80 m linear array composed of 9 microphones spaced in order to optimize the dynamic range. The sound speed is set at $c_0 = 1500$ m/s and the frequency at 2 kHz.

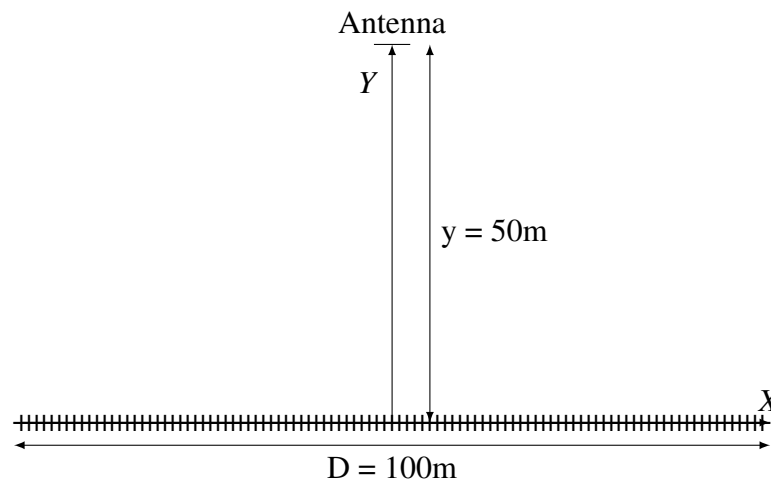
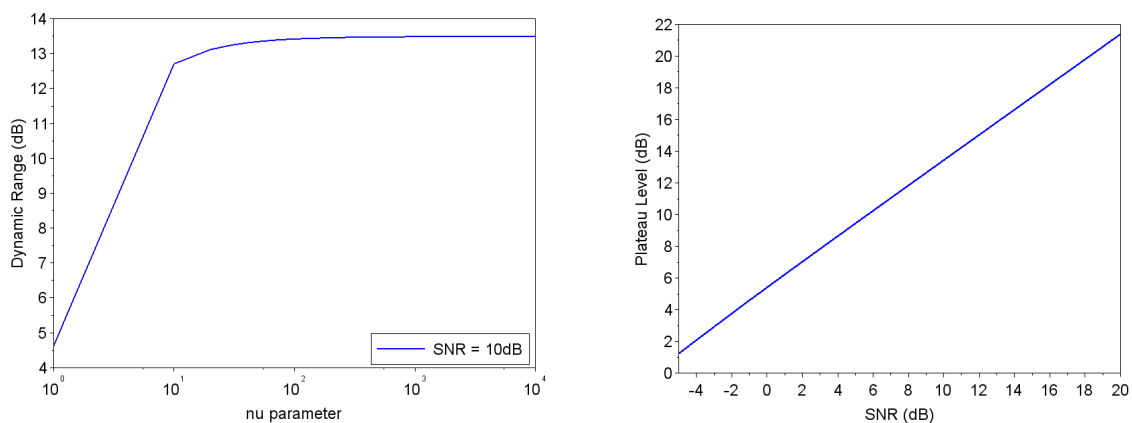


Figure 4: Simulation configuration

Using this configuration three different perturbations are simulated. The first one consists in adding an uncorrelated noise on the CSM. It simulates the electronic noise on the microphones. The second perturbation concerns the propagation model errors. To simulate them, the source is first located between two points of the scan grid and then located ahead or behind the scan grid. Finally extended sources are studied to show how quantification behaves on a source that



(a) Dynamic obtained as a function of ν for a source and an uncorrelated noise (SNR = 10dB) (b) Plateau level in function of the injected noise power

Figure 5: Results for the uncorrelated noise simulation

is spread on several scan grid points.

3.2 Uncorrelated Noise

A noisy antenna can be considered by taking its pressure measurement equals to $\mathbf{p} = \mathbf{p}_s + \mathbf{w}$ with \mathbf{p} the noisy pressure vector over the antenna and \mathbf{w} a noise vector. The noise is a gaussian centered noise with standard deviation σ_w for every microphone. It is uncorrelated between microphones and with the pressure signal \mathbf{p}_s . The CSM is then $C = \mathbf{p}\mathbf{p}^* = \mathbf{p}_s\mathbf{p}_s^* + \sigma_w^2 I_M$ with I_M the identity matrix of size M . The Signal to Noise Ratio (SNR) can be defined as the squared amplitude of the signal at the microphone location over the variance of the noise. So with A the source amplitude and R_s denoting the distance between the source and the center of the array the SNR is given in Eq. (6).

$$SNR = 10 \log_{10} \left(\frac{(A^2/R_s^2)}{\sigma_w^2} \right) \quad (6)$$

In this subsection FBF is performed on the noisy CSM and parameter ν is modified over a wide range of values $[1; 10^4]$. Figure 5a shows the dynamic of the map as a function of the parameter ν for a SNR of 10 dB.

A plateau appears from ν around 50 and the dynamic does not increase anymore beyond this threshold. This plateau is linked to the power of the uncorrelated noise. Indeed, by tracing the level of this plateau as a function of the SNR, Fig. 5b is obtained. A linear dependency is observed between the plateau level and the SNR: the stronger the SNR, the better the dynamic range.

Consequently the dynamic range that can be obtained practically is restricted to a plateau given by the SNR value. So once this plateau is reached it is not useful to go further for the parameter ν . This observation has a strong consequence on the possible use of the method: a generic value of ν is not available in practice because it depends on the SNR.

Finally in this simple case it is possible to achieve better result by denoising the diagonal but

there are limitations such as the determination of the level of noise or the different noise levels on the hydrophones.

3.3 Propagation Model Errors

FBF method is based on a given propagation model. This subsection shows how errors on these parameters can affect FBF quantification results.

Grid Error

The first model error to be studied concerns the position of the source compared to the scan grid. It is possible that the source location does not correspond exactly to a grid point in real conditions (Fig. 6). So the designed steering vector for the grid cannot focus exactly on the source.

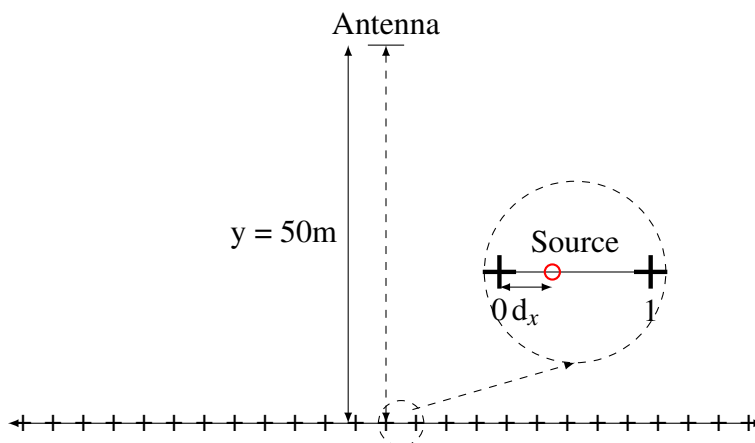


Figure 6: Configuration used to simulate the position error between grid points

In this case five sources are successively simulated from the grid point ($d_x = 0$ m) to the point midway between two grid points ($d_x = 0.5$ m). FBF is performed on each of these sources and Fig. 7 gives the source level estimate for these five processes.

The drop in the source level estimate is all the more pronounced as the source is far from the grid point. Table 1 gives I_{coh} between the source propagation vector and the nearest steering vector. As expected, I_{coh} decreases with the increasing distance between the source and the nearest grid point.

Table 1: I_{coh} for a source located between two grid points

d_x	0 m	0.1 m	0.2 m	0.3 m	0.4 m	0.5 m
I_{coh}	1	0.999	0.997	0.994	0.990	0.985

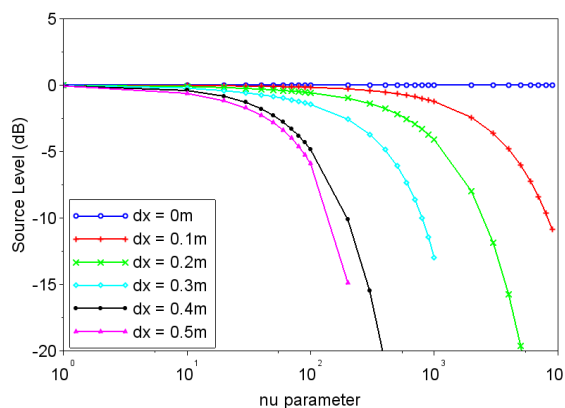


Figure 7: Source level as a function of the parameter ν for grid errors.

$d_x = 0$ m: source on a grid point, $d_x = 0.5$ m: source midway between two grid points

These results show clearly the consequences on the quantification of an inaccurate steering vector: the source level drops indefinitely with an increasing ν even with a value of I_{coh} very close to 1. The drop starts between $\nu = 50$ and $\nu = 1000$ and the source level continuously decreases. In real conditions it is almost impossible to claim a perfect alignment so the quantification performances are degraded. The correct quantification is only given for low ν or when the source is exactly on the grid, reducing the interest of using the method. Nevertheless improvements are possible with for instance a thinner scan grid. This is done in Fig. 8 by placing the source at $d_x = 0.3$ m and testing several step sizes.

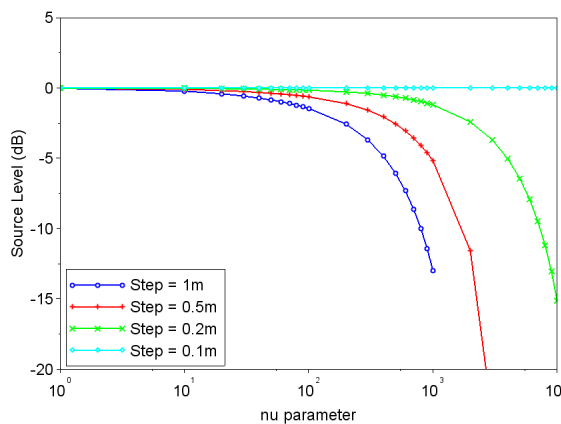


Figure 8: Step size influence on the source level found by FBF

The decrease as a function of the parameter ν is weaker for a smaller step size. It confirms the trend observed above. Note that for a step size thin enough to have a steering vector directly on the source (0.1 m), there is no decrease anymore.

From these simulations we can conclude that there is a clear link between the propagation description through the steering vector and the decrease in estimated quantification.

Distance Error

The second model error studied is the distance between the scan grid and the array. In FBF, as in CBF, it must be fixed and corresponds to the expected distance between the array and the source. Nevertheless it is possible that the source is not exactly located at this distance. Figure 9 illustrates this issue with two examples of sources located ahead and behind the scan grid.

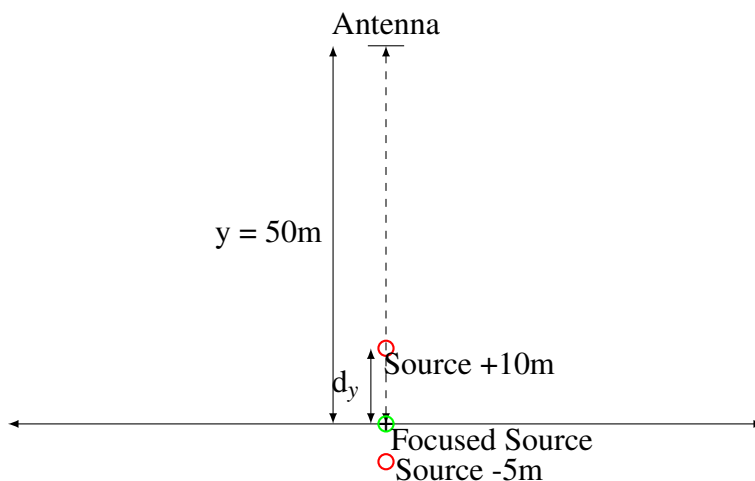


Figure 9: Configuration used to simulate the position error in distance

Five different source positions are studied here: $d_y = 10\text{ m}$ and $d_y = 5\text{ m}$ both ahead and behind the grid and exactly on the grid ($d_y = 0\text{ m}$). The source level is displayed as a function of the parameter ν in Fig. 10.

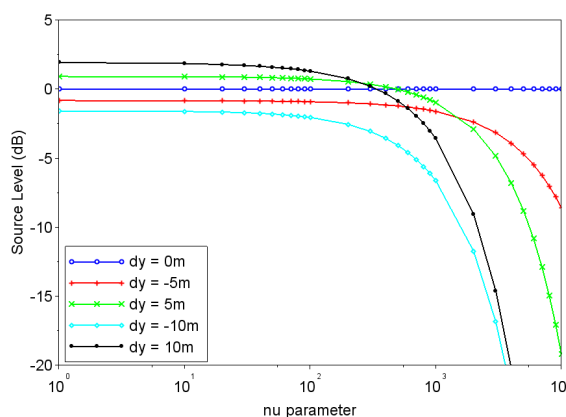


Figure 10: Source level as a function of the parameter ν for different distance errors

One can observe that for small ν , sources located behind the grid are underestimated (up to 2 dB) whereas sources located ahead are overestimated (up to 2.5 dB). Then when ν increases the source level drops starting around $\nu = 100$ for $d_y = \pm 10\text{ m}$, $\nu = 200$ for $d_y = 5\text{ m}$ and $\nu = 1000$ for $d_y = -5\text{ m}$. So the good quantification is never achieved in practice both for low and high ν .

This is another limitation due to the method's need of an accurate propagation model describing the source.

Indeed these results link again steering quality to good quantification as the most decreasing curves are the ones for a low index I_{coh} as shown in Table 2.

Table 2: I_{coh} for the different depth errors

d_y	0 m	-5 m	5 m	-10 m	10 m
I_{coh}	1	0.999	0.999	0.998	0.996

To conclude FBF can quantify accurately in the case of a perfect propagation model used. In practice small model errors always occur and the source level can be significantly underestimated if a too high value is used for ν . The choice of a relevant value for ν becomes then a tricky task.

3.4 Extended sources

This final simulated case addresses the problem of extended sources. Several perfectly correlated sources are simulated on neighbor points (respectively 3 and 5 neighbors around the center of the grid) of the scan grid in order to simulate an extended source. The same neighborhood is defined with uncorrelated sources in order to compare the obtained results. FBF is applied on the different built CSM and Fig. 11 gives the source level computed as a function of the parameter ν . By combining several sources together in this case, the expected power to measure is changed. For the incoherent case it can be easily derived by the sum of the linear power of the sources giving 4.8 dB for 3 sources and 7.0 dB for 5.

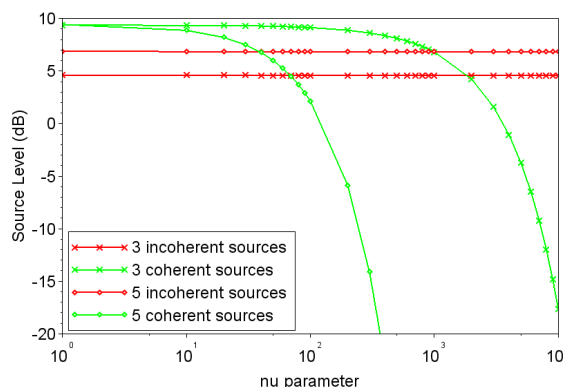


Figure 11: Source level in function of the parameter ν for coherent and incoherent sources

For incoherent sources, the quantification of the source sum is recovered even by increasing ν . So quantification in the presence of several sources is possible with FBF if the sources are incoherent and the propagation model perfectly matches with them. Nevertheless this is only a global quantification that takes into account the three sources together. This is a limitation

coming from the CBF that assumes that only one source is present at a time within the scanned grid.

For coherent sources, a similar decrease is observed as for the steering mismatch. Indeed from $\nu \simeq 100$ the maximum value of the map that corresponds to the source level starts to decrease strongly. Moreover the more the source is extended, the bigger the effect is. It is actually another type of "model error".

This issue is problematic because in practical conditions almost every source is localized on several grid points. Physically speaking, a source located on a single grid point means that this source is infinitely thin and perfectly aligned with the grid which is impossible, particularly at low frequencies.

Consequently FBF is not suited to quantify extended sources but it can estimate globally the acoustic power of several incoherent sources together even if they are closely spaced.

4 EXPERIMENTAL APPROACH

4.1 Experimental Setups

The goal of the experimental part is to validate the results observed during the simulation step. Two experimental setups are used and presented in Fig. 12. The first one (Fig. 12a) has been used within LUG 2 project in the LVA anechoic room. An intensimetry measurement giving a quantification reference is available and then a MicrodB's HDCam antenna is placed in front of a baffled source at a distance of 12 cm.

The second one (Fig. 12b) has been conducted in the LMFA windtunnel in the FRAE funded SEMAFOR project. It aims at validating the simulation results on a realistic setup. A turbulent air flow is impinging a NACA 12 airfoil. Aeroacoustic noise is created from the interaction of the air flow with both the airfoil leading edge and trailing edge. This case contains complex and distributed sources that describe a more realistic application than the first one.

4.2 Experimental Results

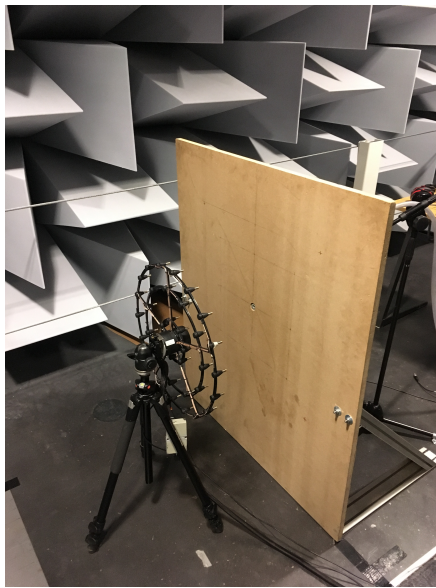
Baffled Source

The goal is to compare the quantification obtained by FBF for different ν values. It has to be noted that the displayed quantification value correspond to the maximum value obtained within the map for each case.

In Fig 13 the quantification error defined by the difference between the intensimetry reference and the source level is displayed for different ν as a function of the frequency. Since the intensimetry technique has a ± 2 dB uncertainty, quantification results are considered acceptable if they lie between the two horizontal dotted lines of Fig 13.

For an increasing ν , the quantification results lower which confirms the simulation results. However contrary to the simulation results, problems occur for very low ν : for $\nu = 10$ the quantification result is already outside the 2 dB limits. Thus the limitations identified in Section 3 are even more serious limitations in practice.

As proposed in simulation, a computation on a thinner grid is performed to try mitigating the quantification losses. The results obtained for grids that vary from 1 cm to 1 mm step size are presented in Fig. 14.

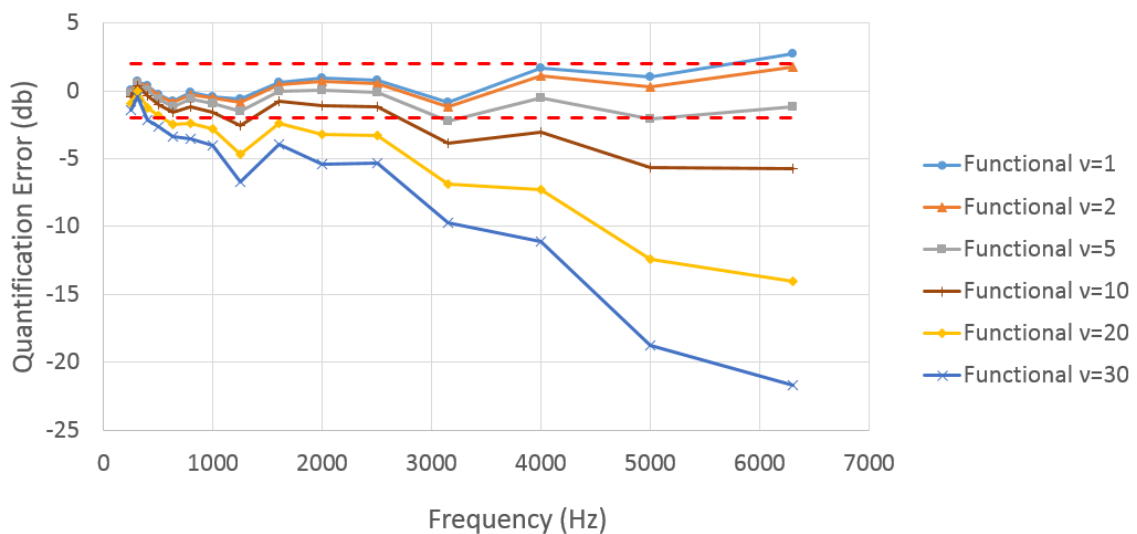


(a) Baffled source



(b) NACA 12 Airfoil

Figure 12: Experimental setups

Figure 13: Gap between source level with FBF and the intensimetry reference (for $v = 1, 2, 5, 10, 20, 30$)

Contrary to the simulation, experimentally the gain between the different grids is not visible. It can be explained by the presence of other errors that disturb stronger the quantification preventing an improvement by this simple solution.

To conclude, this experimental setup confirms the results obtained in the different simulations: the growth of the exponent v causes a decreasing in the quantification level obtained. Nevertheless there is a major difference: the quantification errors start earlier ($v = 10$) than in simulation ($v > 100$).

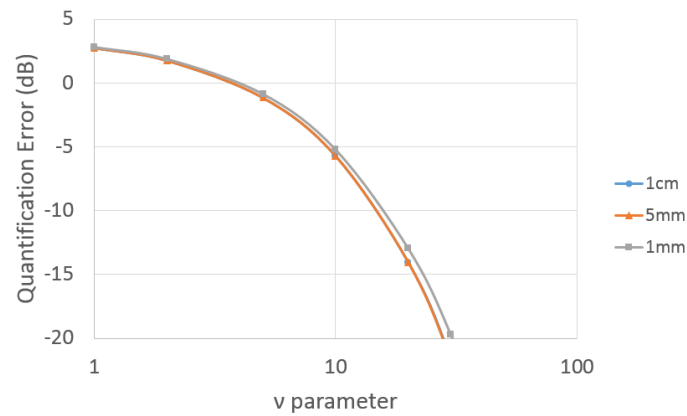


Figure 14: Quantification error as a function of ν (for step size = 1cm, 5mm, 1mm)

Aeroacoustic Case

The different maps computed for the aeroacoustic experiment are given for different ν (1,2,10,50) in Fig. 15 at 1 kHz.

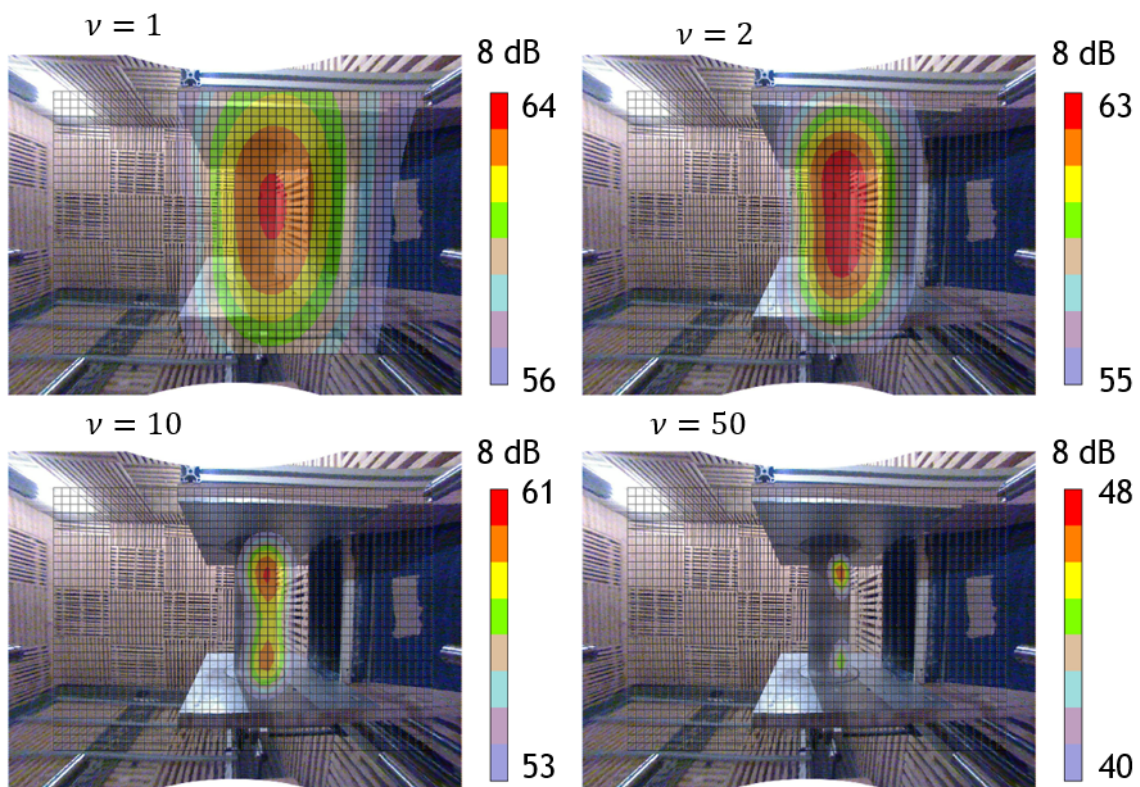


Figure 15: FBF localization results for the aeroacoustic case at 1kHz ($\nu = 1, 2, 10, 50$)

Then the maximum value of the map, corresponding to the strongest source, is traced as a function of ν up to $\nu = 50$ in Fig. 16.

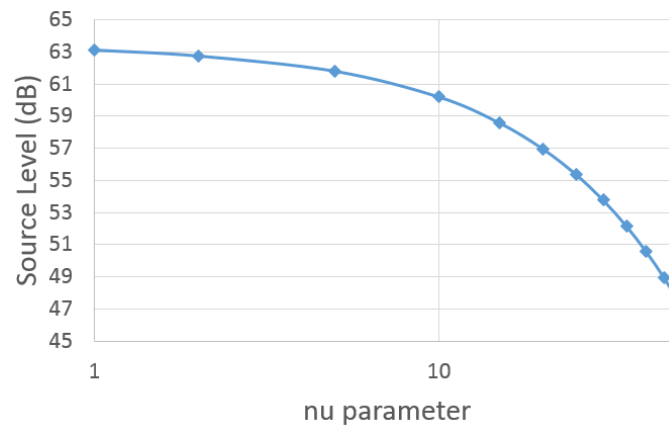


Figure 16: Source level as a function of ν

The decreasing of the source level observed confirms again the simulations results. However the decreasing happens even earlier than in the previous experiment (since the first ν tested) which is due to the complexity of the studied sources and the propagation errors.

5 CONCLUSION

Functional Beamforming is a technique to perform acoustic source localization based on Conventional Beamforming. Its usefulness concerning acoustic source localization with an efficient computation time is clear. In this contribution the reliability of its acoustic power measurements is assessed.

The impacts of uncorrelated added noise and model errors are studied using simulations. It shows first that the method is constrained in its use in the presence of noise: the parameter ν is limited to a certain value above which there is no more gain. Then the precision of the steering vector has a strong importance on the quantification performance. Indeed, when it is not perfectly aligned with the one describing the propagation, a decrease of the estimated source power is noticed when the parameter of the method ν increases. A decrease is also noticed in the case of extended sources. However it can be reduced by computing the map on a thinner grid.

Then experimental data are processed. At first a baffled source with an intensimetry reference shows clearly the decrease as a function of ν . However this decrease happens earlier than in simulation. Moreover contrary to the simulations the thinner grid cannot improve the results. Then a more complex aeroacoustic case is investigated which gives satisfying localization results but enhances the method difficulties to quantify as the decrease starts even earlier than in the previous experiment. This can be explained by the fact that this time all the errors are put together along others not even considered during the simulation step.

To conclude the Functional Beamforming suffers limitations to quantify acoustic sources accurately. Indeed having the good acoustic power level contradicts with the fact that ν has to be increased to enhance localization results. These limitations are due to the perfect matching between model and reality which is not respected. In order to go further in the theoretical understanding of these effects, investigations on methods developed by Lagunas [6] or Pisarenko

[10] in the domain of spectral analysis could be carried out.

References

- [1] Z. Chu, Y. Yang, and L. Shen. “Resolution and quantification accuracy enhancement of functional delay and sum beamforming for three-dimensional acoustic source identification with solid spherical arrays.” *Mechanical Systems and Signal Processing*, 88, 274–289, 2017.
- [2] R. Dougherty. “Functional beamforming for aeroacoustic source distributions.” *AIAA paper*, 3066, 2014.
- [3] H. Cox, R. Zeskind, and M. Owen. “Robust adaptive beamforming.” *IEEE Transactions on Acoustics, Speech, and Signal Processing*, 35(10), 1365–1376, 1987.
- [4] J. Capon. “High-resolution frequency-wavenumber spectrum analysis.” *Proceedings of the IEEE*, 57(8), 1408–1418, 1969.
- [5] J. Li, P. Stoica, and Z. Wang. “On robust Capon beamforming and diagonal loading.” *IEEE Transactions on Signal Processing*, 51(7), 1702–1715, 2003.
- [6] M. Lagunas, M. Santamaria, A. Gasull, and A. Moreno. “Maximum likelihood filters in spectral estimation problems.” *Signal Processing*, 10(1), 19–34, 1986.
- [7] R. Merino-Martinez, M. Snellen, and D. Simons. “Functional beamforming applied to full scale landing aircraft.” In *6th Berlin beamforming conference, Berlin*. 2016.
- [8] R. Merino-Martínez, M. Snellen, and D. G. Simons. “Functional beamforming applied to imaging of flyover noise on landing aircraft.” *Journal of Aircraft*, 53(6), 1830–1843, 2016.
- [9] S. Vorobyov, A. Gershman, and Z. Luo. “Robust adaptive beamforming using worst-case performance optimization: a solution to the signal mismatch problem.” *IEEE Transactions on Signal Processing*, 51(2), 313–324, 2003.
- [10] V. Pisarenko. “On the Estimation of Spectra by Means of Non-linear Functions of the Covariance Matrix.” *Geophysical Journal of the Royal Astronomical Society*, 28(5), 511–531, 1972.